Camera Self-Calibration from Two Views with a Common Direction

Yingna Su[1,2], Xinnian Guo[1,2] and Yang Shen[3]
[1]*College of Information Engineering, Suqian University, Suqian, China*
[2]*Suqian Key Laboratory of Visual Inspection and Intelligent Control, Suqian University, Suqian, China*
[3]*Industrial Technology Research Institute, Suqian University, Suqian, China*

Keywords: Camera Self-Calibration, Gravity Direction, Homography Constraints, Principal Point Estimation.

Abstract: Camera calibration is crucial for enabling accurate and robust visual perception. This paper addresses the challenge of recovering intrinsic camera parameters from two views of a planar surface, that has received limited attention due to its inherent degeneracy. For cameras equipped with Inertial Measurement Units (IMUs), such as those in smartphones and drones, the camera's *y*-axes can be aligned with the gravity direction, reducing the relative orientation to a one-degree-of-freedom (1-DoF). A key insight is the general orthogonality between the ground plane and the gravity direction. Leveraging this ground plane constraint, the paper introduces new homography-based minimal solutions for camera self-calibration with a known gravity direction. we derive 2.5- and 3.5-point camera self-calibration algorithms for points in the ground plane to enable simultaneous estimation of the camera's focal length and principal point. The paper demonstrates the practicality and efficiency of these algorithms and comparisons to existing state-of-the-art methods, confirming their reliability under various levels of noise and different camera configurations.

1 INTRODUCTION

In the field of computer vision, the calibration of cameras plays a fundamental role in enabling accurate and robust visual perception. Planar structures are ubiquitous in man-made environments and have found extensive utility in various geometric model estimation tasks. Zhang et al. (Zhang, 2000) employed a known planar target to derive a closed-form solution for the camera calibration problem. Fitzgibbon (Fitzgibbon, 2001) introduced a minimal solver for the estimation of two-view homography with consistent distortion. Kukelova and Pajdla (Kukelova et al., 2015) presumed varying distortions between two cameras and formulated algorithms for estimating corresponding homography and distortion parameters. Nonetheless, the challenge of recovering intrinsic camera parameters from two views of a planar surface has received limited attention, primarily due to its degeneracy in the context of most algorithms (Nistér, 2004).

Recent research by Ding et al. (Ding et al., 2022) has demonstrated the feasibility of resolving this problem when the two views share a common direction. This finding bears particular relevance, given the prevalence of smartphones, tablets, and camera systems in applications such as automobiles and unmanned aerial vehicles (UAVs), which commonly feature IMUs capable of measuring the gravitational vector. Given an uncalibrated smart device, e.g., a smart phone, we can capture the images and the corresponding IMU data which can be used to measure the gravity direction. As shown in (Kukelova et al., 2010; Guan et al., 2018), the relationship between the axes of the camera and the IMU are usually 0°, 90° or 180°. In this case, the rotation between the camera and the IMU of smart devices can be known without calibrating the camera and the IMU. We can align y-axes of the camera with the gravity direction, reducing relative orientation to 1-DoF rotation around

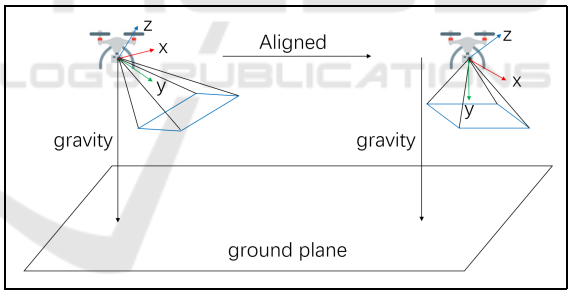

Figure 1: The *y*-axis of the camera is orthogonal to the ground plane after being aligned with the gravity direction.

Su, Y., Guo, X. and Shen, Y.
Camera Self-Calibration from Two Views with a Common Direction.
DOI: 10.5220/0012438100003660

In *Proceedings of the 19th International Joint Conference on Computer Vision, Imaging and Computer Graphics Theory and Applications (VISIGRAPP 2024) - Volume 3: VISAPP*, pages 680-685
ISBN: 978-989-758-679-8; ISSN: 2184-4321

the gravity direction (Fig. 1). A crucial insight is the general orthogonality between the ground plane and the gravity direction. This assumption is fulfilled for many man-made environments, and has been successfully used in many computer vision tasks (Dibene et al., 2023; Li et al., 2023). Leveraging this ground plane constraint, we propose new homography-based minimal solutions for camera self-calibration with the known gravity direction. The proposed framework is depicted in Fig. 2 The main contributions of this paper are:

(i) By exploiting the ground plane assumption, we show that the Euclidean homography matrix has special properties which allows us to derive new constraints and solve the homography-based camera self-calibration problem efficiently.

(ii) Based on the new homography-based constraints, we derive 2.5-point algorithms for points in the ground plane to estimate the focal length of the camera.

(iii) Moreover, we propose a 3.5-point algorithm to estimate the focal length and principal point coordinates of the camera simultaneously.

2 OUR APPROACH

2.1 Homography-Based Constraints

Suppose two image points $\mathbf{m} = [u, v, 1]^\top$ and $\mathbf{m}' = [u', v', 1]^\top$ are given for a point on a plane in the 3D space with respect to two camera frames. The Euclidean homography matrix $\mathbf{H}$ that transforms one into the other satisfies

$$\lambda \mathbf{K}^{-1}\mathbf{m}' = \mathbf{H}\mathbf{K}^{-1}\mathbf{m}, \tag{1}$$

where λ is a scaling factor, and $\mathbf{K}$ is the camera intrinsic matrix. The Euclidean homography matrix $\mathbf{H}$ is related to the rotation matrix $\mathbf{R}$, the translation matrix $\mathbf{T}$, the distance d from the camera frame to the target plane, and the normal $\mathbf{N}$ of the plane according to

$$\mathbf{H} = \mathbf{R} - \frac{1}{d}\mathbf{T}\mathbf{N}^\top. \tag{2}$$

Since the gravity direction can be calculated from the IMU data, without loss of generality, we can align the y-axes of the cameras with the gravity direction (Fig. 1). After alignment, the rotation transformation matrix of two camera views reduces from 3-DoF to 1-DoF and can be represented as

$$\mathbf{R}_y = \begin{bmatrix} \cos\theta & 0 & \sin\theta \\ 0 & 1 & 0 \\ -\sin\theta & 0 & \cos\theta \end{bmatrix}. \tag{3}$$

Applying the rotations to the normalized image points, then Eq. (1) becomes

$$\lambda \mathbf{R}_2^\top \mathbf{K}^{-1}\mathbf{m}' = \mathbf{H}_y \mathbf{R}_1^\top \mathbf{K}^{-1}\mathbf{m}, \tag{4}$$

with

$$\mathbf{H}_y = \mathbf{R}_y - \mathbf{t}\mathbf{n}^\top, \tag{5}$$

where $\mathbf{R}_1$,$\mathbf{R}_2$ are the rotation matrices of two cameras for the alignment, $\mathbf{t} = [t_x, t_y, t_z]^\top$ and $\mathbf{n}$ are the translation and plane parameters after the alignment. Based on the assumption that the ground planes are orthogonal to the gravity direction, the plane normal n is equal to $[0\ 1\ 0]^\top$ when the points lie in a horizontal plane. Then Eq. (5) can be formulated as

$$\begin{aligned} \mathbf{H}_y &= \begin{bmatrix} \cos\theta & 0 & \sin\theta \\ 0 & 1 & 0 \\ -\sin\theta & 0 & \cos\theta \end{bmatrix} - \begin{bmatrix} t_x \\ t_y \\ t_z \end{bmatrix} [0\ 1\ 0] \\ &= \begin{bmatrix} \cos\theta & -t_x & \sin\theta \\ 0 & 1-t_y & 0 \\ -\sin\theta & -t_z & \cos\theta \end{bmatrix}. \end{aligned} \tag{6}$$

Obviously $\mathbf{H}_y$ obeys 4 constraints:

$$h_4 = 0,\ \ h_6 = 0,\ \ h_1 - h_9 = 0,\ \ h_3 + h_7 = 0, \tag{7}$$

where h_i are the elements of the matrix $\mathbf{H}_y$. These constraints allow us to solve minimal solutions for camera self-calibration more efficiently.

2.2 Unknown Focal Length(2.5-point)

For most modern CCD and CMOS cameras, it is reasonable to assume unit aspect ratio and that the principal point coincides with the image centerEq.(Hartley and Li, 2012). In this case, the only unknown intrinsic camera parameter is the focal length f. We propose a 2.5-point algorithm for estimating f.

In general, Eq. (1) can be written as

$$\lambda \mathbf{m}' = \mathbf{G}\mathbf{m}, \tag{8}$$

where $\mathbf{G}$ transforms the image points. Given one point correspondence $(\mathbf{m}, \mathbf{m}')$, Eq. (8) can also be written as

$$\begin{bmatrix} 0 & 0 & 0 & -u & -v & -1 & v'u & v'v & v' \\ u & v & 1 & 0 & 0 & 0 & -u'u & -u'v & -u' \end{bmatrix} \mathbf{g} = 0,$$

$$\mathbf{g} = [g_1\ g_2\ g_3\ g_4\ g_5\ g_6\ g_7\ g_8\ g_9]^\top, \tag{9}$$

where $g_1, g_2, ..., g_9$ are the elements of the 2D homography matrix $\mathbf{G}$. Each point correspondence gives two linearly independent constraints. By stacking the constraints for κ point correspondences,Eq. (9) leads to a system of equations of the form

$$\mathbf{A}\mathbf{g} = 0, \tag{10}$$

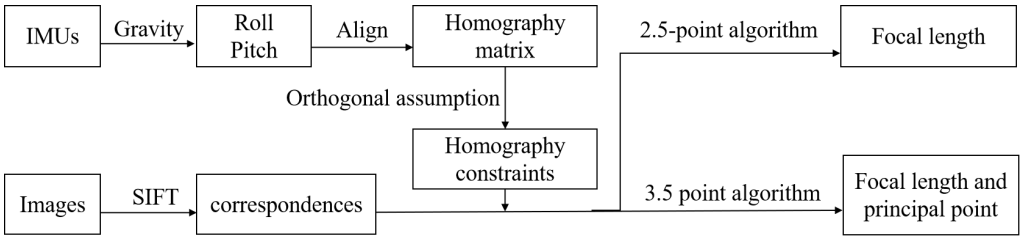

Figure 2: The overall framework of the proposed method.

where $\mathbf{A}$ is a $2\kappa \times 9$ matrix. Then $\mathbf{g}$ and the 2D homography matrix $\mathbf{G}$ can be found as the null space of $\mathbf{A}$. With 2.5 point correspondences (note that we still need to use three point correspondences, but only need one equation from the last correspondence), the general solution of $\mathbf{g}$ in Eq. (10) is a 4-dimensional null space which can be written as

$$\mathbf{g} = \alpha\mathbf{g}_a + \beta\mathbf{g}_b + \gamma\mathbf{g}_c + \mathbf{g}_d, \tag{11}$$

where α, β, γ are the coefficients. Based on Eq. (4) and Eq. (8), the Euclidean homography matrix $\mathbf{H}_y$ can be formulated as

$$\mathbf{H}_y = \mathbf{R}_2^\top \mathbf{K}^{-1}\mathbf{G}\mathbf{K}\mathbf{R}_1. \tag{12}$$

Let $\mathbf{K} = \mathrm{diag}(f, f, 1)$, $\mathbf{K}^{-1} = \mathrm{diag}(1/f, 1/f, 1)$. Substituting Eq. (11) into Eq. (12) we can parameterize $\mathbf{H}_y$ using $\{\alpha, \beta, \gamma, f\}$. Then substituting this formulation into constraints Eq. (7), we obtain 4 polynomial equations in 4 unknowns $\{\alpha, \beta, \gamma, f\}$:

$$\mathbf{a}_i[1, \alpha, \beta, \gamma, f, \alpha f, \beta f, \gamma f, f^2, \alpha f^2, \beta f^2, \gamma f^2]^\top = 0, \tag{13}$$

where $\{\mathbf{a}_i | i = 1, 2, 3, 4\}$ are coefficients. The system of equations Eq. (13) can be solved using the Gröbner basis method (Cox et al., 2006). For more details about the Gröbner basis method and the polynomial eigenvalue solution we refer the reader to (Kukelova et al., 2012; Larsson et al., 2017b; Larsson et al., 2017a; Larsson et al., 2018). There are up to 4 real solutions. Negative solutions of f can also be abandoned.

2.3 Unknown Focal Length and Principal Point(3.5-point)

However, sometimes the principal point may not coincide with the image center. In this case, the unknown camera intrinsic parameters are the unknown focal length f and the principal point (u_0, v_0). Let

$$\mathbf{K} = \begin{bmatrix} f & 0 & u_0 \\ 0 & f & v_0 \\ 0 & 0 & 1 \end{bmatrix}, \mathbf{K}^{-1} = \begin{bmatrix} 1/f & 0 & -u_0/f \\ 0 & 1/f & -v_0/f \\ 0 & 0 & 1 \end{bmatrix}. \tag{14}$$

We derive a 3.5-point algorithm to estimate the camera intrinsic parameters. With 3.5 point correspondences, the general solution of $\mathbf{g}$ in Eq. (10) is a 2-dimensional null space which can be written as

$$\mathbf{g} = \alpha\mathbf{g}_a + \mathbf{g}_b. \tag{15}$$

Substituting Eq. (14) and Eq. (15) into Eq. (12) we can parameterize $\mathbf{H}_y$ using $\{\alpha, f, u_0, v_0\}$. Then substituting this formulation into constraints Eq. (7), we obtain 4 polynomial equations in 4 unknowns $\{\alpha, f, u_0, v_0\}$:

$$\mathbf{b_i}[1, \alpha, f, u_0, v_0, \alpha f, \alpha u_0, \alpha v_0, f u_o, f v_0, u_0 v_0, \cdots \\ \alpha f u_0, \alpha f v_0, \alpha u_0 v_0, f^2, u_0^2, v_0^2, \alpha f^2, \alpha u_0^2, \alpha v_0^2]^\top = 0, \tag{16}$$

where $\{\mathbf{b_i} | i = 1, 2, 3, 4\}$ are coefficients. Here we recommend using an automatic generator to solve the system of polynomial equations, e.g. , (Larsson et al., 2017a). We obtain a Gauss-Jordan elimination template of size 79×91, and there are up to 12 real solutions.

3 EXPERIMENTS

We choose the following setup to generate the synthetic data for the self-calibration evaluation. It contains two image sequences. The simulated cameras of both sequences have the same parameters: the focal length f_g of the camera is set to 3442 pixels, and the coordinates of the principal point (u_g, v_g) is set to $(2016, 1512)$. The image resolution of the first sequence is 4032×3024, i.e., the principal point of the camera coincides with the image center. The image resolution of the second sequence is 3225×2419 which indicates that the principal point does not locate at the center of the image. 100 3D points are distributed on the ground plane which is orthogonal to the image plane of the first view. Each 3D point is observed by two camera views to generate an image pair. This is similar to (Fraundorfer et al., 2010; Saurer et al., 2017; Ding et al., 2022). We generate 1,000 pairs of images for each sequence to evaluate the performance. The relative focal length error is de-

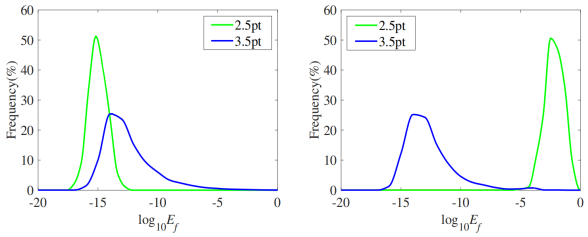

(a) the first sequence (b) the second sequence

Figure 3: Histograms of the relative focal length error E_f distribution for 10,000 runs with the first and the second image sequences, respectively.

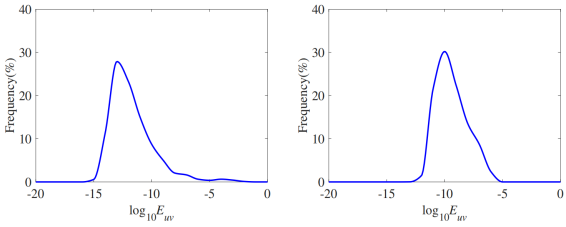

(a) the first sequence (b) the second sequence

Figure 4: Histograms of the principal point error E_{uv} distribution for 10,000 runs with the first and the second image sequences, respectively.

fined as

$$E_f = |f_e - f_g|/f_g, \tag{17}$$

where f_e denotes the estimated focal length and f_g is the ground truth. The principal point error is formulated as

$$E_{uv} = \sqrt{(|(u_e - u_g)|/u_g) * (|(v_e - v_g)|/v_g)}, \tag{18}$$

where (u_e, v_e) denotes the estimated coordinates of the principal point and (u_g, v_g) is the true one.

3.1 Numerical Precision

Figure 3 shows the histograms of the relative focal length error E_f of the proposed algorithms for 10,000 runs with the first and the second image sequences, respectively. '2.5pt' denoteS the 2.5-point algorithms using the Gröbner basis solution. '3.5pt' denotes the 3.5-point algorithms using the Gauss-Jordan elimination template of size 79×91. The error distribution of Fig. 3(a) shows that the 2.5-point algorithm performs as expected for the focal length estimation when the principal point of the camera coincides with the image center. The stability of 3.5-point algorithm is not as good as the 2.5-point case, but it does not contain large errors and is sufficient for real applications. As shown in Fig. 3(b), the 3.5-point algorithm is more reliable than the 2.5-point algorithm when the principal point of the camera does not locate at the center of the image. Figure 4 shows the principal point error E_{uv} of the 3.5-point algorithm for 10,000 runs with the first and the second image sequences, respectively. As shown, our method is efficient and robust in estimating the principal point of the camera on both of the image sequences.

3.2 Stability of the Solutions Compared to Other Methods

In this section we compare the proposed methods with the state of the arts. '6pt' denotes the two-view 6-point algorithm proposed in (Kukelova et al., 2017). '4pt' denotes the 4-point homography based algorithm proposed in (Ding et al., 2022). Because we still need to sample 3 and 4 points in practice, we use SVD to compute the null space with 3 and 4 points, respectively. These algorithms are evaluated under increased level of image noise (point location) from 0 to 1 pixel. In addition, the gravity direction measured by the accelerometers is not perfect in real environment. Thus we also simulate the noisy case with increased roll, pitch noise (gravity direction) and constant image noise of 0.5 pixel standard deviation. The max standard deviation of the (roll, pitch) noise is set to 0.5°, because smart phone IMUs typically have noise of less than 0.5° (Sweeney et al., 2014). Note that for our algorithms we use the noisy roll, pitch angles to compute the full rotation.

Figure 5 shows the median focal length error of the first image sequence (the first row) and the second image sequence (the second row) with increased image noise (the left column), roll noise (the middle column) and pitch noise (the right column), respectively. As expected, the proposed 2.5-point algorithm performs better than the other ones under perfect IMUs data and the 3.5-point algorithm can also achieve promising results for estimating the focal length of camera when the principal point of the camera locates at the center of the image (as shown in Fig. 5(a)). Figure 5(b) shows that the proposed 3.5-point algorithm is more accurate than the other three methods when the principal point of the camera does not coincide with the image center. The 6pt algorithm is not influenced by the roll and pitch noise because it does not need IMUs data. Overall, we can see that the proposed 2.5- and 3.5-point algorithms are slightly better than the other methods on focal length estimation when the principal point of the camera does and does not coincide with the image center, respectively.

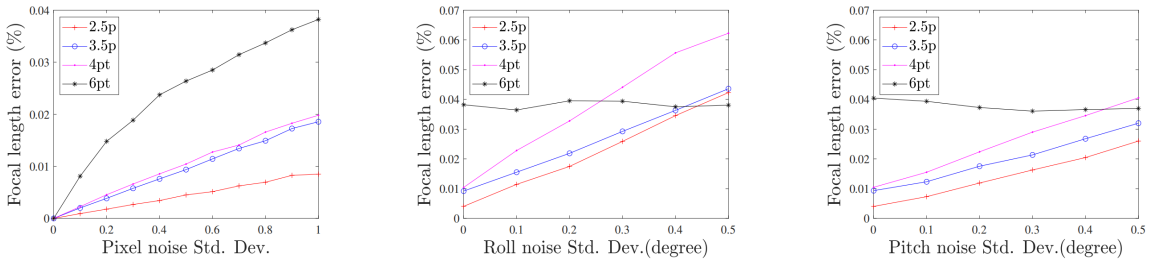

(a) the first image sequence

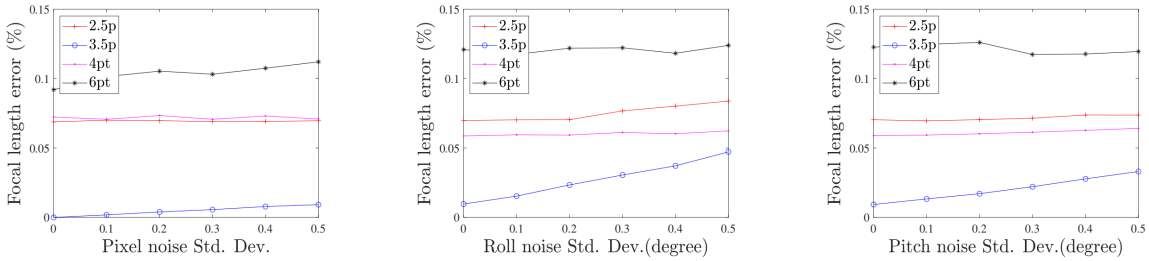

(b) the second image sequence

Figure 5: Boxplot of relative focal length error. The results of the first column are with the increased image noise from 0 to 1 pixel. The results of the second column are with the increased roll noise from 0 to 0.5° and the constant image noise of 0.5 pixel. The results of the last column are with the increased pitch noise from 0 to 0.5° and the constant image noise of 0.5 pixel.

Table 1: The principal point error E_{uv} of the 3.5-point algorithm with the synthetic data for 10,000 runs under both image sequences.

		the first sequence		the second sequence	
		mean	median	mean	median
Image noise	0	1.153 e-09	1.8685 e-13	1.2959 e-09	1.8688 e-13
	0.5	0.0396	0.012	0.0405	0.0119
	1.0	0.0704	0.0241	0.0692	0.0237
Roll noise	0.1	0.0496	0.0193	0.0462	0.0187
	0.3	0.1060	0.0457	0.1134	0.0534
	0.5	0.1503	0.0666	0.1537	0.0782
Pitch noise	0.1	0.0471	0.0192	0.0460	0.0184
	0.3	0.0705	0.0305	0.0687	0.0295
	0.5	0.0919	0.0438	0.0877	0.0433

3.3 Evaluation of the Principal Point

To our best knowledge, no homography-based two view method has been performed to estimate the principal point. So we only give the statistical results of our method without the comparisons to other methods. Table 1 gives the principal point error E_{uv} of the 3.5-point algorithm with the synthetic data for 10,000 runs under both image sequences. Similarly, we evaluate the 3.5-point algorithm under increased level of image noise and roll, pitch noise. The third and the fourth column show the results of the first image sequence (the principal of the camera coincides with the image center). The fifth and the sixth column give the results of the second image sequence (the principal point does not locate at the image center). The third to the fifth rows show the principal point error E_{uv} with the increased image noise from 0 to 1 pixel. The sixth to the eighth rows show the results with the increased roll noise from 0 to 0.5 degree and the constant image noise of 0.5 pixel standard deviation. The last three rows shows the results with the increased pitch noise from 0 to 0.5 degree and the constant image noise of 0.5 pixel. As shown, the proposed method can achieve efficient results for the principal point estimation under different noise cases and sequences.

In general, based on the simulation experiments we find that the proposed 2.5- and 3.5-point algorithms are comparable to the existing methods for the focal length and the principal point estimation under different noise cases. To the best of our knowledge, good IMUs today can have noise levels of around 0.06 degrees in the computed angles (Fraundorfer et al., 2010). In this case, our algorithms are practical and can be used as alternative algorithms on camera self-calibration pipelines for smart phones and tablets.

4 CONCLUSION

This paper proposes a self-calibration method for estimating camera focal length and principal point based on the orthogonality assumption and homography constraints. Leveraging IMU data and the orthogonality assumption, new homography constraints are derived in this paper. The 2.5-point and 3.5-point methods for estimating camera focal length and principal point are presented. Thanks to the simplified constraints, the algorithm in this paper not only exhibits superior performance compared to alternative approaches but also ensures high efficiency. We believe that the method proposed in this paper can serve as an alternative algorithm for camera self-calibration in intelligent vehicle applications, further enhancing the performance of intelligent vehicle systems.

ACKNOWLEDGEMENTS

The authors would like to thank the editor and the anonymous reviewers for their critical and constructive comments and suggestions. This work is supported by Suqian science and technology plan project under No. K202233, K202229, K202231, H202117 and Suqian Natural Science Foundation (No. M202305).

REFERENCES

Cox, D. A., Little, J., and O'shea, D. (2006). *Using algebraic geometry*, volume 185. Springer Science & Business Media.

Dibene, J. C., Min, Z., and Dunn, E. (2023). General planar motion from a pair of 3d correspondences. In *Proceedings of the IEEE/CVF International Conference on Computer Vision*, pages 8060–8070.

Ding, Y., Barath, D., Yang, J., and Kukelova, Z. (2022). Relative pose from a calibrated and an uncalibrated smartphone image. In *Proceedings of the IEEE/CVF Conference on Computer Vision and Pattern Recognition*, pages 12766–12775.

Fitzgibbon, A. (2001). Simultaneous linear estimation of multiple view geometry and lens distortion. In *Proceedings of the 2001 IEEE Computer Society Conference on Computer Vision and Pattern Recognition. CVPR 2001*.

Fraundorfer, F., Tanskanen, P., and Pollefeys, M. (2010). A minimal case solution to the calibrated relative pose problem for the case of two known orientation angles. In *The European Conference on Computer Vision (ECCV)*.

Guan, B., Yu, Q., and Fraundorfer, F. (2018). Minimal solutions for the rotational alignment of imu-camera systems using homography constraints. *Computer vision and image understanding*.

Hartley, R. and Li, H. (2012). An efficient hidden variable approach to minimal-case camera motion estimation. *IEEE transactions on pattern analysis and machine intelligence*.

Kukelova, Z., Bujnak, M., and Pajdla, T. (2010). Closed-form solutions to minimal absolute pose problems with known vertical direction. In *Asian Conference on Computer Vision*.

Kukelova, Z., Bujnak, M., and Pajdla, T. (2012). Polynomial eigenvalue solutions to minimal problems in computer vision. *IEEE Transactions on Pattern Analysis and Machine Intelligence*.

Kukelova, Z., Heller, J., Bujnak, M., and Pajdla, T. (2015). Radial distortion homography. In *The IEEE Conference on Computer Vision and Pattern Recognition (CVPR)*.

Kukelova, Z., Kileel, J., Sturmfels, B., and Pajdla, T. (2017). A clever elimination strategy for efficient minimal solvers. In *The IEEE Conference on Computer Vision and Pattern Recognition (CVPR)*.

Larsson, V., Åström, K., and Oskarsson, M. (2017a). Efficient solvers for minimal problems by syzygy-based reduction. In *The IEEE Conference on Computer Vision and Pattern Recognition (CVPR)*.

Larsson, V., Astrom, K., and Oskarsson, M. (2017b). Polynomial solvers for saturated ideals. In *The IEEE International Conference on Computer Vision (ICCV)*.

Larsson, V., Oskarsson, M., Åström, K., Wallis, A., Kukelova, Z., and Pajdla, T. (2018). Beyond gröbner bases: Basis selection for minimal solvers. In *The IEEE Conference on Computer Vision and Pattern Recognition (CVPR)*.

Li, H., Zhao, J., Bazin, J.-C., Kim, P., Joo, K., Zhao, Z., and Liu, Y.-H. (2023). Hong kong world: Leveraging structural regularity for line-based slam. *IEEE Transactions on Pattern Analysis and Machine Intelligence*.

Nistér, D. (2004). An efficient solution to the five-point relative pose problem. *IEEE transactions on pattern analysis and machine intelligence*.

Saurer, O., Vasseur, P., Boutteau, R., Demonceaux, C., Pollefeys, M., and Fraundorfer, F. (2017). Homography based egomotion estimation with a common direction. *IEEE transactions on pattern analysis and machine intelligence*.

Sweeney, C., Flynn, J., and Turk, M. (2014). Solving for relative pose with a partially known rotation is a quadratic eigenvalue problem. *3DV*.

Zhang, Z. (2000). A flexible new technique for camera calibration. *IEEE Transactions on pattern analysis and machine intelligence*, 22.